Acta Cryst. (1993). A**49**, 27-35

The Complex Perovskite-Related Superstructure $Ba_2Fe_2O_5$ Solved by HREM and CIP

BY X. D. ZOU AND S. HOVMÖLLER

Department of Structural Chemistry, Stockholm University, S-106 91 Stockholm, Sweden

M. PARRAS AND J. M. GONZÁLEZ-CALBET

Departamento de Química Inorgánica, Facultad de C. Químicas, Universidad Complutense, 28040-Madrid, Spain

M. VALLET-REGÍ

Departamento de Química Inorgánica y Bioinorgánica, Facultad de Farmacia, Universidad Complutense, 28040-Madrid, Spain

AND J. C. GRENIER

Laboratoire de Chimie du Solide du CNRS, Université de Bordeaux I, 33405 *Talence CEDEX, France*

(*Received* 16 *August* 1991; *accepted* 28 *November* 1991)

Abstract

Barium ferrite $Ba_2Fe_2O_5$ is a complex perovskite-related structure. The crystal is monoclinic $P2_1/c$, with $a = 6.969(1)$, $b = 11.724(1)$, $c = 23.431(5)$ Å, $\beta = 98.74(1)°$. The composition of one unit cell is $Ba_{28}Fe_{28}O_{70}$. The structure was solved using a combination of high-resolution electron microscopy (HREM), crystallographic image processing (CIP) and electron diffraction. The structure can be described as a perovskite with 14 oxygen positions unoccupied with respect to the ABO_3 stoichiometry in the monoclinic unit cell. These positions can be identified from the potential map obtained by HREM and CIP. They form two linear groups. Seven of them lie on a line along $[476]_m$ (corresponding to $[110]_c$ of perovskite), while the seven other symmetry-related positions lie along $[4\bar{7}6]_m$ (corresponding to $[101]_c$ of perovskite).

Introduction

Since the early work of Erchark, Fankuchen & Ward (1946), the Ba-Fe-O system has been extensively studied (Ichida, 1973; Negas & Roth, 1969; González-Calbet, Parras, Vallet-Regí & Grenier, 1990; Grenier, Wattiaux, Pouchard, Hagenmuller, Parras, Vallet, González-Calbet & Alario, 1989). Particular attention has been devoted to the $BaFeO_{2.5}$ perovskite-related phase since X-ray powder diffraction studies led to contradictory results. This phase was considered by several authors (Gallagher, MacChesney & Buchanan, 1965; Zanne, 1973) to be isostructural with brownmillerite $Ca_2Fe_2O_5$ (Bertaut, Blum & Sagnières, 1959), which has an orthorhombic cell with $a = 5.83$, $b = 16.98$, $c = 5.54$ Å. On the other hand, a triclinic unit cell with $a = 4.049$, $b = 4.049$, $c = 4.139$ Å, $\alpha = 89°41'$, $\beta = 89°41'$, $\gamma = 92°48'$ was suggested by considering some of the diffraction peaks attributed to superstructure reflections (Mori, 1965). Yet another orthorhombic unit cell was proposed; similar to the above-mentioned orthorhombic cell, but with the c axis doubled (Luccinni, Meriani & Minichelli, 1970).

To elucidate the true symmetry of the unit cell of $Ba_2Fe_2O_5$, an electron diffraction (ED) study was undertaken by Parras, Vallet-Regí, González-Calbet, Alario, Grenier & Hagenmuller (1987). They concluded that this phase has monoclinic symmetry with the space group $P2_1/c$. The monoclinic unit cell parameters are multiples of a cubic perovskite subcell. The relation between the monoclinic (m) and cubic (c) perovskite unit cells is

$$\begin{bmatrix} a_m \\ b_m \\ c_m \end{bmatrix} = \begin{bmatrix} 1 & \bar{1} & \bar{1} \\ 0 & 2 & \bar{2} \\ 4 & 3 & 3 \end{bmatrix} \begin{bmatrix} a_c \\ b_c \\ c_c \end{bmatrix}.$$

According to this, the monoclinic cell contains 28 cubic perovskite subcells, leading to a $Ba_{28}Fe_{28}O_{70}$ composition for this phase. A Rietveld refinement (Rietveld, 1967) with all Ba and Fe atoms located as in the corresponding f.c.c. AO_3' stacking, and a random distribution of the oxygen vacancies, agreed well with X-ray powder data. Only the weak diffraction peaks, owing to the ordering of oxygen vacancies, could not be explained. The unit-cell parameters were refined from the X-ray powder diffraction data to be $a = 6.969(1)$, $b = 11.724(1)$, $c = 23.438(5)$ Å, $\beta = 98.74(1)°$ (Parras, Fournes, Grenier, Pouchard, Calbet, Vallet & Hagenmuller, 1990). Chemical analysis showed that all Fe atoms are +III (Parras, Vallet-Regí, González-Calbet, Alario, Grenier & Hagenmuller, 1987).

0108-7673/93/010027-09$06.00

A Mössbauer spectroscopy study (Parras, Fournes, Grenier, Pouchard, Calbet, Vallet & Hagenmuller, 1990) indicated the following environments for Fe^{III}: three octahedral sites, three tetrahedral ones and one site with fivefold coordination. The chemical formula can be written

$$Ba_{28}[FeO_3]_{12}[FeO_2]_{12}[FeO_{2.5}]_4 \equiv Ba_{28}Fe_{28}O_{70} \equiv Ba_2Fe_2O_5.$$

Although we have information about symmetry, unit-cell dimensions and metal-atom positions of $Ba_2Fe_2O_5$, the techniques applied are not sufficient to solve the superstructure of this material completely, *i.e.* to locate the unoccupied oxygen positions.

It is often quite difficult to solve inorganic structures with very large unit cells, such as that of $Ba_{28}Fe_{28}O_{70}$. High-resolution transmission electron microscopy (HREM) combined with crystallographic image processing (CIP) has been used to solve the structure of complex metal oxides such as $Na_3Nb_{12}O_{31}F$ (Li & Hovmöller, 1988) and $Cs_xNb_{54}(O, F)_{146}$ ($x \leq 8$) (Wang, Hovmöller, Kihlborg & Sundberg, 1988). The three-dimensional structure of the perovskite-related $Ca_4Fe_2Ti_2O_{11}$ was also obtained by CIP (Hovmöller, Zou, Wang, González-Calbet & Vallet-Regí, 1988). With this technique the crystallographic structure-factor phases are determined experimentally from the computed Fourier transform of a digitized electron micrograph. Crystallographic symmetry constraints on amplitudes and phases are imposed and this may compensate for the distortions in the image caused by multiple scattering, crystal tilt and electron optical effects.

We applied CIP to HREM images of $Ba_2Fe_2O_5$ to solve its crystal structure.

Experimental

Stoichiometric amounts of $BaCO_3$ and α-Fe_2O_3 were heated at 1373 K for 24 h under nitrogen. The obtained homogeneous brown product was slowly cooled under nitrogen. Powder X-ray characterization was performed on a Siemens D-500 diffractometer equipped with a graphite monochromator in the diffracted beam and using Cu $K\alpha$ radiation. HREM was carried out on a 4000EX JEOL electron microscope fitted with a double-tilting top-entry goniometer stage (±25°), operated at 400 kV.

HREM images were first selected on an optical diffractometer. Thin areas near the edge with sharp diffraction spots were digitized on a Joyce Loebl Microdensitometer 6. The raster size was 40 × 40 μm, 256 × 256 points were scanned for each area. For an image with 400 000 times magnification a 40 μm raster size corresponds to a 1 Å sampling interval in the specimen, which is sufficiently fine to preserve the resolution up to at least 2.4 Å. The digitization and the calculation of Fourier transforms of the images were as described earlier (Hovmöller, Sjögren, Farrants, Sundberg & Marinder, 1984). Amplitudes and phases were obtained from the Fourier transforms calculated on a VAX 11/750 computer.

The amplitude part of the Fourier transform was displayed on a colour graphics display. It was compared to the corresponding electron diffraction pattern. Images that were not taken at exactly the Scherzer-focus conditions showed a dark ring [contrast transfer function (CTF) crossover] on the graphics. When such crossover was found, the phases for the reflections outside this ring were shifted by 180°.

The reflections from the basic perovskite lattice are very strong. We applied the direct methods as developed by Hauptman & Karle (1953) for checking the phases of the strong triple relation $0\bar{4}0$, 027 and $02\bar{7}$.

For the space group $P2_1/c$, the amplitude and phase relations between symmetry-related reflections $0kl$ are:

$$k + l = 2n: \quad |F(0kl)| = |F(0\bar{k}\bar{l})|, \; \alpha(0kl) = \alpha(0\bar{k}\bar{l});$$

$$k + l = 2n + 1: \; |F(0kl)| = |F(0\bar{k}\bar{l})|, \quad \alpha(0kl) = \alpha(0\bar{k}\bar{l}) + 180°.$$

These symmetry constraints were imposed on amplitudes and phases obtained from HREM and CIP. Because the structure is centrosymmetric, phases were then set to 0° if they were closer to 0 than to 180°; otherwise they were set to 180°.

The coordinates for all the atoms in the monoclinic unit cell were deduced from the coordinates of those in the cubic perovskite and the matrix relating the monoclinic and cubic unit cells. The coordinates for the four unoccupied oxygen positions were found from the potential map obtained by HREM and CIP.

Results

From the HREM images it can be seen that $Ba_2Fe_2O_5$ forms large well ordered crystals. Images taken along [100] (Fig. 1) show unit-cell repeats of 23.2 (23.43 × sin 98.7°) by 11.7 Å. A direct intuitive interpretation of these images is not possible due to the complexity of the structure and changes of the appearance with crystal thickness. In the thinnest areas near the edge only the basic pseudohexagonal pattern with $a = 3.3$. and $b = 3.4$ Å is seen (Fig. 2). Further away from the edge, as the crystal becomes thicker, a different pattern emerges. The details of this pattern change from one part of the crystal to another but it is always clear that the unit cell is 23.2 by 11.7 Å. In many areas of intermediate thickness, one can see an arrangement of a checker-board type, with two bright and two dark blocks per unit cell.

The Fourier transform of a small area with the hexagonal pattern (marked 'a' in Fig. 2) shows only six strong reflections, which form a hexagonal lattice representing the $[1\bar{1}\bar{1}]$ projection of a basic perovskite structure. In the Fourier transform of a small area with the checker-board pattern (marked 'b' in Fig. 2), there are many weaker reflections besides the six strong reflections. The six strong reflections can be

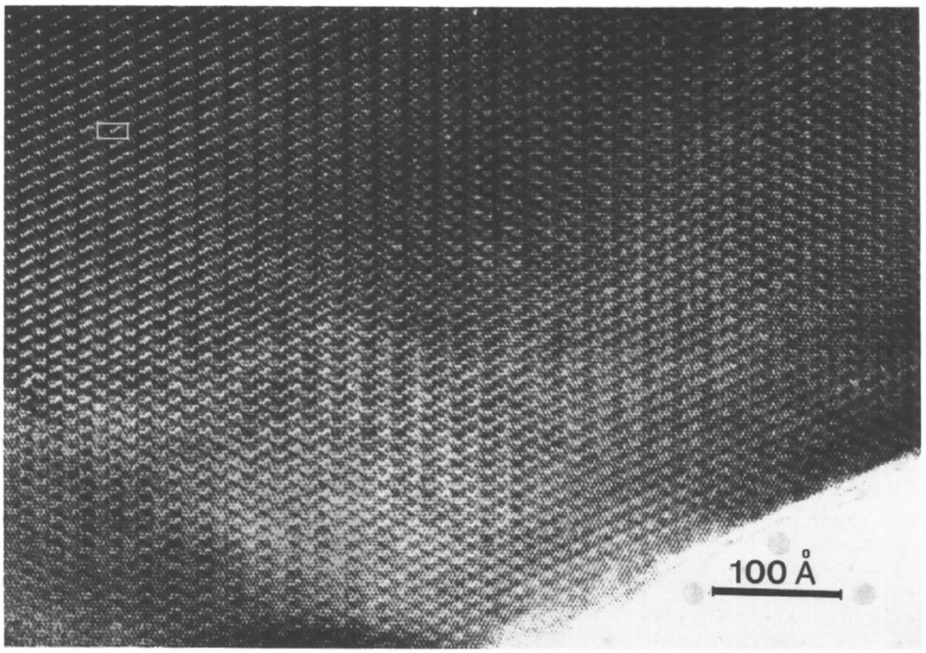

Fig. 1. A HREM image of $Ba_2Fe_2O_5$ taken along the *a* axis. The crystal is well ordered over a large area, but the contrast changes with specimen thickness.

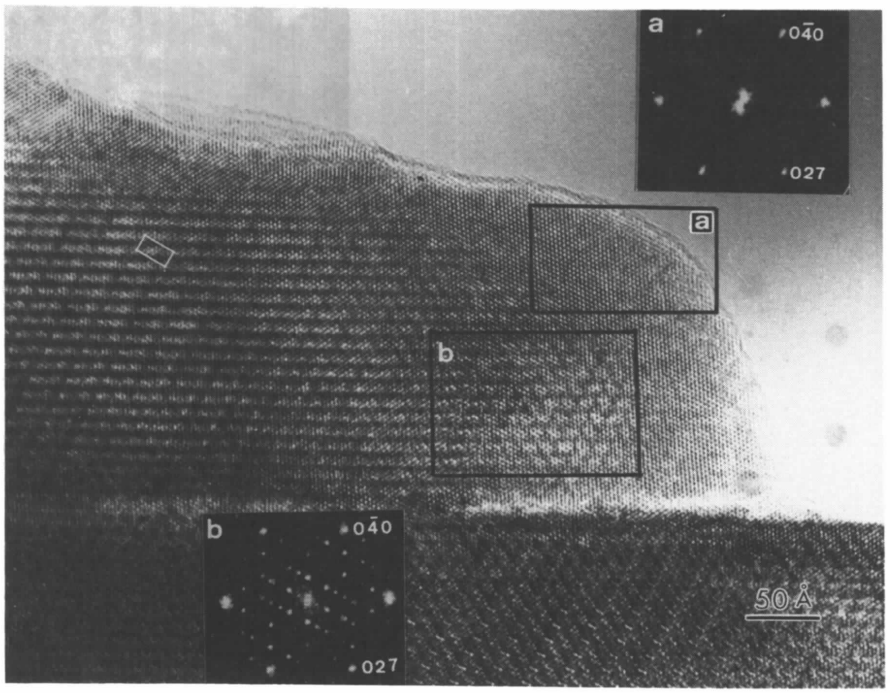

Fig. 2. The scanned image of $Ba_2Fe_2O_5$. A hexagonal pattern appears at the very thin edge (marked 'a'), while a checker-board-like pattern appears in the thicker areas (marked 'b'). Insets: calculated Fourier transforms of areas a and b, respectively.

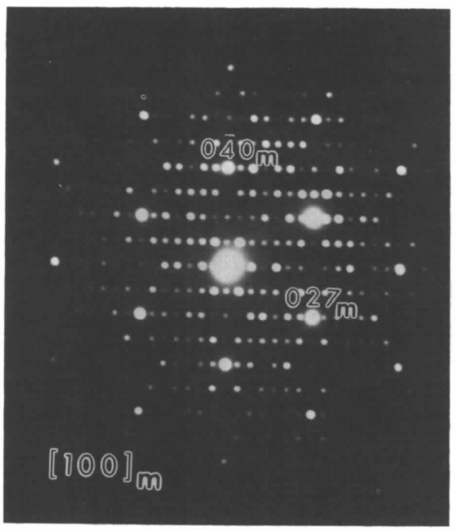

(*a*)

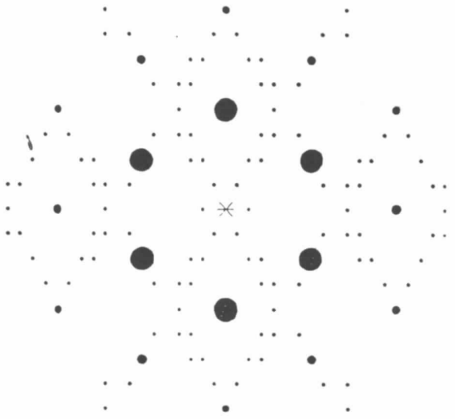

(*b*)

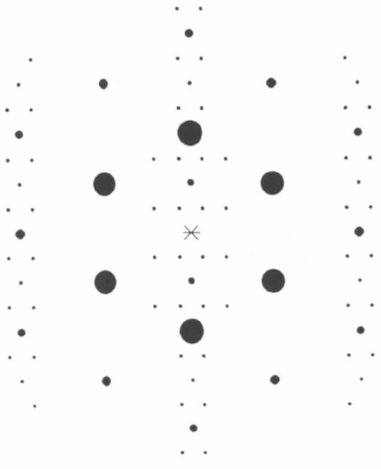

(*c*)

Fig. 3. Electron diffraction pattern of $Ba_2Fe_2O_5$ along the [100] zone axis. (*a*) The observed pattern; the subscript *m* refers to the monoclinic cell. (*b*) The calculated pattern from (the correct) model 1. (*c*) The calculated pattern from (the incorrect) model 2.

indexed as $0,\pm4,0$, $0,\pm2,\pm7$ in the monoclinic unit cell. They represent the basic perovskite structure, while the weak reflections represent the superstructure. The amplitudes and phases of the Fourier transform of the thicker area were used for further processing.

In the [100] electron diffraction patttern (Fig. 3*a*), the pseudohexagonal lattice of strong reflections extends to very high resolution (less than 1 Å). That means that all the atom positions, especially the metal-atom positions, are close to those of the basic perovskite.

In the Fourier transform of the scanned area (Fig. 4), there is an elliptical dark ring at about 4 Å resolution as marked in Fig. 4(*b*). This is the CTF crossover. We compensated for this by adding 180° to the phases of the reflections outside the ring. The amplitudes and phases before and after this CTF correction and after imposing symmetry are listed in Table 1. For

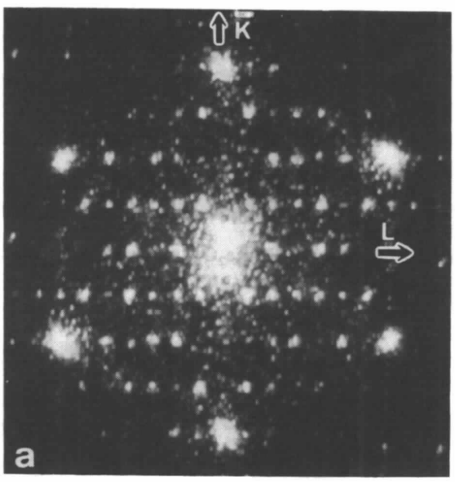

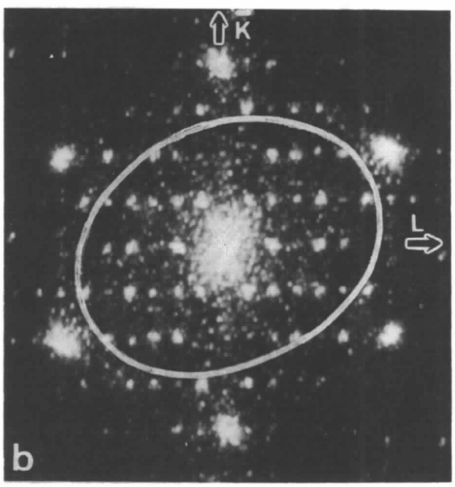

Fig. 4. The Fourier transform of the scanned image. The dark ellipse in (*a*) (marked by a white ring in *b*) is caused by a crossover of the CTF.

Table 1. *Amplitudes and phases* (°) *before* (I) *and after* (II) *CTF correction and after imposing symmetry* (III)

	Amplitudes		Averaged	Phases I		Phases II		Phases III	
h k l	$0\bar{k}l$	$0kl$	amplitudes	$0\bar{k}l$	$0kl$	$0\bar{k}l$	$0kl$	$0\bar{k}l$	$0kl$
0 0 2	560	-	560	24	-	24	-	0	-
0 0 4	223	-	223	215	-	215	-	180	-
0 0 6	25	-	25	20	-	20	-	0	-
0 0 8	40	-	40	82	-	262	-	180	-
0 1 1	833	1014	923	195	172	195	172	180	180
0 1 2	360	395	377	40	214	40	214	0	180
0 1 3	303	76	189	351	57	351	57	0	0
0 1 4	118	68	93	36	265	36	265	0	180
0 1 5	184	114	149	135	206	135	26	180	180
0 1 6	160	157	158	332	273	332	93	0	180
0 1 7	78	38	58	162	247	342	67	0	0
0 1 8	148	18	83	31	185	211	5	180	0
0 2 0	192	-	192	355	-	355	-	0	-
0 2 1	13	25	19	129	70	129	70	180	0
0 2 2	541	221	381	190	183	190	183	180	180
0 2 3	140	178	159	87	46	87	46	180	0
0 2 4	51	13	32	53	198	53	18	0	0
0 2 5	292	121	206	79	71	79	251	0	180
0 2 6	−91	−48	-	269	113	-	-	-	-
0 2 7	2282	1088	1685	170	64	350	244	0	180
0 2 8	108	−12	48	5	79	185	259	180	180
0 3 1	192	246	219	5	335	185	155	180	180
0 3 2	95	82	88	30	202	210	22	180	0
0 3 3	212	26	119	358	244	178	64	180	180
0 3 4	117	−12	52	189	190	9	10	0	180
0 3 5	110	9	59	237	293	57	113	0	0
0 3 6	139	21	80	88	315	268	135	0	180
0 4 0	1352	-	1352	189	-	9	-	0	-
0 4 1	42	39	40	207	11	27	191	180	0
0 4 2	114	22	68	205	8	25	188	0	0
0 4 3	12	−7	2	90	167	270	347	0	180
0 4 4	30	17	23	269	349	89	169	0	0

centrosymmetric crystals all phases are 0 or 180°. The deviation from these values, the amplitude-weighted phase residual, was 27.8° and the amplitude R_{sym} value was 42%. The phases of the reflections at highest resolution were hard to assign. Possibly some of them were affected by a second CTF crossover.

Potential maps were calculated from the amplitudes and phases for $P1$ symmetry, before and after correcting for the CTF [Figs. 5(*a*) and (*b*), respectively]. The positions of the peaks changed very much after the CTF correction. The contrast of the original map (Fig. 5*a*) was almost reversed, since the phases of the three strongest reflections $0\bar{4}0$, $0\bar{2}7$ and 027 were all shifted by 180°. There are blocks of stronger peaks at the corners and centres of the unit cells, but the atomic details are blurred (Fig. 5*b*). After the crystallographic symmetry was imposed ('Averaged amplitudes' and 'Phases III' as listed in Table 1), a new potential map was calculated (Fig. 5*c*).

The map after imposing the symmetry shows 4 by 7 nearly equally spaced peaks in each unit cell, corresponding to columns of metal atoms of the perovskite structure. The map can be interpreted such that each of the 28 peaks corresponds to a column of alternating Ba and Fe atoms. However, the heights of the peaks are not equal. Blocks of 2 by 3 stronger peaks are seen around (00) and $(\frac{11}{22})$, while other peaks are weaker. These differences are interpreted as a variation in the oxygen content around metal atoms. There are seven unique peaks in the unit cell. The three strongest peaks must be the octahedral sites. The two weakest peaks are interpreted as tetrahedral sites. The remaining two peaks, according to Mössbauer data, must correspond to one tetrahedral and one square pyramidal site, although they have similar heights. Depending on which of the two intermediate peaks is five-coordinated, two different structure models emerge. All atoms of $Ba_2Fe_2O_5$ are considered to remain at the positions derived from the cubic perovskite. The 14 unoccupied oxygen positions were found for both models.

In both models, the 14 unoccupied oxygen positions form two groups of seven lying on straight lines (Fig. 6). We define them as vacancy lines in comparison with the basic perovskite. In the projection, the centres of the two lines are at $(0\frac{1}{2})$ and $(\frac{1}{2}0)$, respectively. In model 1, one vacancy line lies parallel to [76], while the other line is parallel to $[\bar{7}6]$ (Fig. 6*a*). In model 2, both lines are parallel to the [01] axis (Fig. 6*b*). Although in terms of vacancy positions the two models appear very different, in terms of coordinations of Fe atoms they are very similar. The only variation is an interchange between two neighbouring four- and five-coordinated Fe atoms (Figs. 6*a*, *b*).

To establish which of the two models is correct, we compared calculated and observed diffraction intensities. Intensities for $0kl$ reflections were

calculated for both models (Figs. 3*b*, *c*). They were compared with the electron diffraction pattern (Fig. 3*a*). Model 2 with vacancy lines parallel to [01] gave intensities (Fig. 3*c*) very different from the observed data. Model 1 with vacancy lines parallel to [76] and [$\bar{7}$6] gave intensities (Fig. 3*b*) in close agreement with the observed data. From this we concluded that model 1 is the correct structure model.

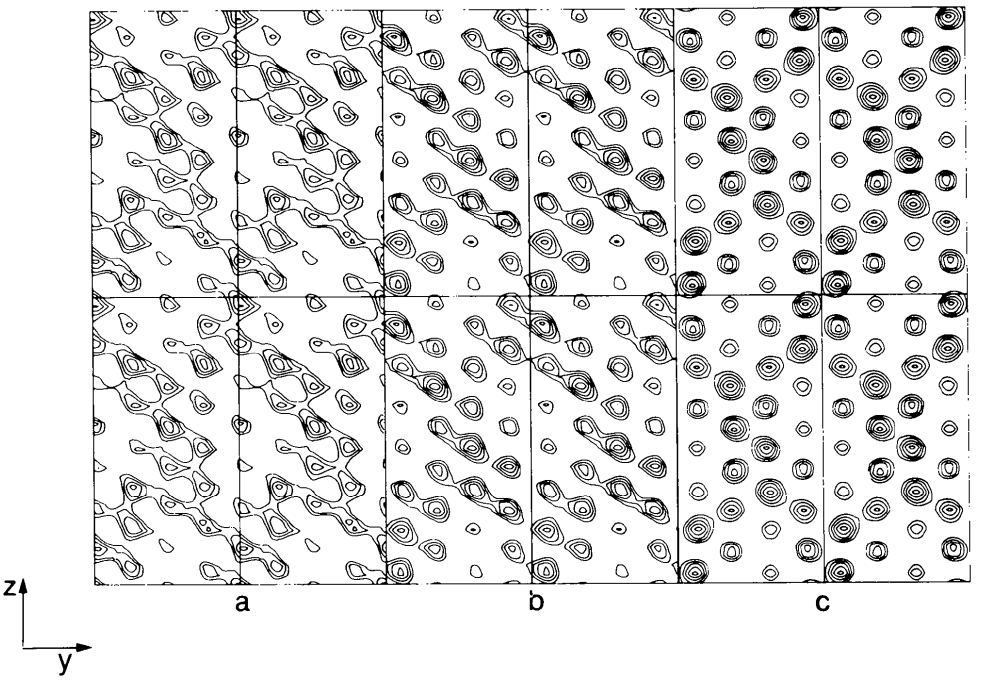

Fig. 5. Potential maps of $Ba_2Fe_2O_5$ calculated by CIP. (*a*) Before CTF correction. (*b*) After CTF correction. (*c*) After CTF correction and imposition of the crystallographic symmetry.

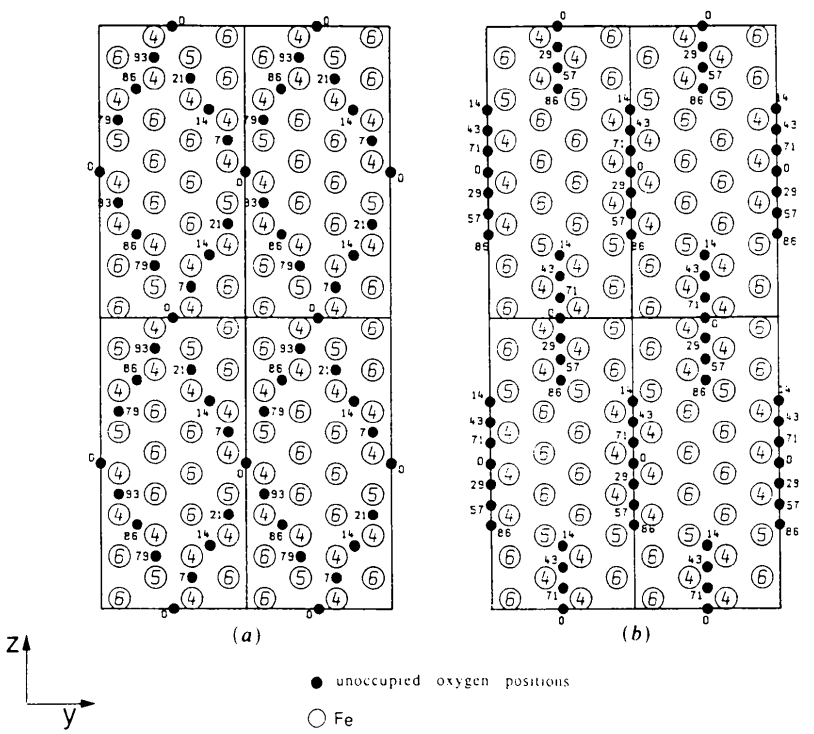

Fig. 6. The [100] projection for the two models showing the location of the unoccupied oxygen positions (●) with their fractional *x* coordinates (multiplied by 100) and the Fe coordination numbers. (*a*) With ● along [76] and [$\bar{7}$6]. This model fits well with the experimental electron diffraction intensities. (*b*) With ● along [01]. This model does not fit with the experimental electron diffraction intensities.

The structure model of $Ba_2Fe_2O_5$ is shown in a projection along the *a* axis (Fig. 7) and in a stereographic representation (Fig. 8). The atomic coordinates for the unique metal and O atoms and the coordination numbers for the Fe atoms are listed in Table 2.

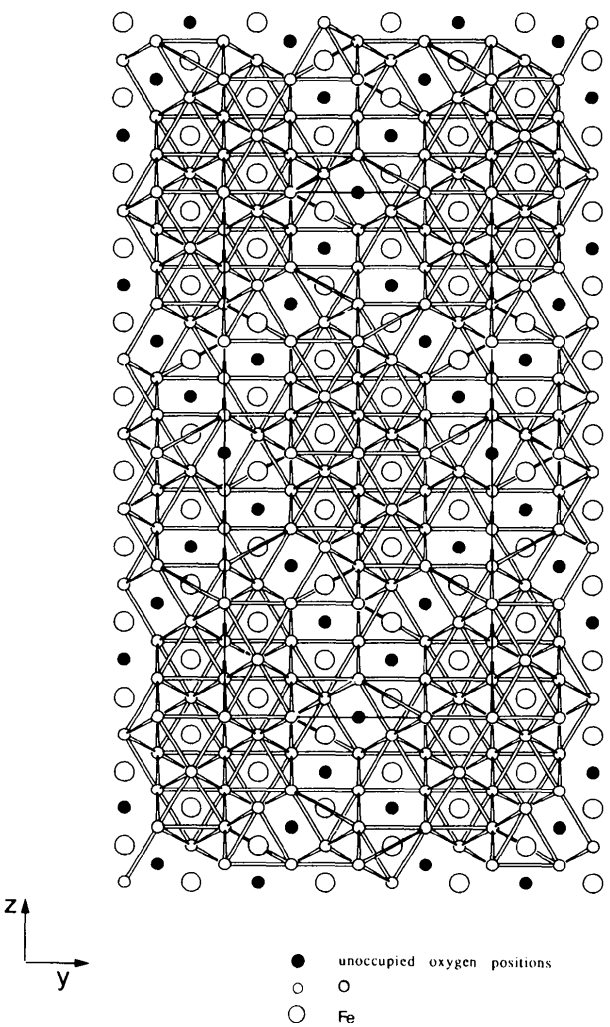

Fig. 7. A projection of $Ba_2Fe_2O_5$ along the *a* axis.

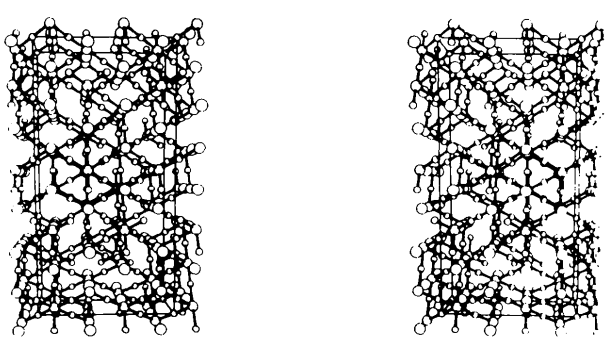

Fig. 8. A stereographic model of $Ba_2Fe_2O_5$. The Ba atoms are drawn larger than the Fe atoms.

Table 2. *Fractional atomic coordinates for* $Ba_2Fe_2O_5$ *and coordination number (CN) for the* Fe *atoms*

All atoms are in general positions, except O1 (marked with *), which is in the 2(*a*) position.

Atom	*x*	*y*	*z*	CN
Ba1	0.3571	0.1250	0.0357	
Ba2	0.7857	0.1250	0.1786	
Ba3	0.2143	0.1250	0.3214	
Ba4	0.6429	0.1250	0.4643	
Ba5	0.0714	0.1250	0.6071	
Ba6	0.5000	0.1250	0.7500	
Ba7	0.9286	0.1250	0.8929	
Fe1	0.8571	0.1250	0.0357	6
Fe2	0.2857	0.1250	0.1786	6
Fe3	0.7143	0.1250	0.3214	4
Fe4	0.1429	0.1250	0.4643	4
Fe5	0.5714	0.1250	0.6071	5
Fe6	0.0000	0.1250	0.7500	4
Fe7	0.4286	0.1250	0.8929	6
O1*	0.0000	0.0000	0.0000	
O2	0.0000	0.2500	0.0000	
O3	0.7143	0.0000	0.0714	
O4	0.7143	0.2500	0.0714	
O5	0.0714	0.1250	0.1071	
O6	0.4286	0.0000	0.1429	
O7	0.4286	0.2500	0.1429	
O8	0.1429	0.0000	0.2143	
O9	0.1429	0.2500	0.2143	
O10	0.5000	0.1250	0.2500	
O11	0.8571	0.0000	0.2857	
O12	0.5714	0.0000	0.3571	
O13	0.5714	0.2500	0.3571	
O14	0.2857	0.0000	0.4286	
O15	0.2857	0.2500	0.4286	
O16	0.3571	0.1250	0.5357	
O17	0.2143	0.1250	0.8214	
O18	0.6429	0.1250	0.9643	

The vacancy lines in the structure of $Ba_2Fe_2O_5$ are parallel to the plane perpendicular to the *a* axis and along $[476]_m$ and $[4\bar{7}6]_m$. These correspond to $[110]_c$ and $[101]_c$ in the basic perovskite. The central atoms of the lines are located at $(0\frac{1}{2}0)$ and $(00\frac{1}{2})$, respectively. The different vacancy lines are at different heights and at an angle of 60° with respect to each other. They form an intricate weave. Tetrahedra are located on both sides of the vacancy lines. At each end of a vacancy line there is a square pyramid. It connects with two tetrahedra that are related to another non-parallel vacancy line and that are close to the centre of the line.

Discussion

The $Ba_2Fe_2O_5$ compound has 126 atoms in the unit cell. All the atoms are located in general positions, except one O atom at the special position (0,0,0). Thus 14 unique metal positions and 17 unique oxygen positions have to be determined. In the monoclinic [100] projection, the crystal is oriented such that the metal atoms form 28 columns of alternating Ba and Fe atoms, while each of the 70 O atoms forms a

column by itself. With some previous knowledge about perovskite, it becomes possible to derive three-dimensional atomic positions from a single two-dimensional projection. If the resolution had been high enough (about 1.6 Å), oxygen positions would have been seen directly by HREM and CIP. With lower resolution, as in this case, the atomic positions of the O atoms can only be obtained from geometrical considerations, namely half-way between neighbouring Fe atoms.

It is worth mentioning that the amplitudes and phases, as obtained from the Fourier transforms of HREM images, are those present in the images. These would have been identical to the amplitudes and phases of the crystallographic structure factors, had the images been ideal undistorted magnifications of the projected potential distribution of the structure. However, they are not. Several factors distort the image. These are: multiple scattering within the crystal, electron optical distortions (defocus, astigmatism and beam tilt), crystal tilt and noise. With CIP, the crystallographic structure factors are reconstructed.

After imposition of the symmetry, the three reflections $0\bar{4}0$, $02\bar{7}$ and 027 of $Ba_2Fe_2O_5$ forming a triple relation have phases 0, 180 and 0°, respectively (Table 1). Their phases sum to 180°. Since we have scanned the negative film, the density is reversed compared with that of the real image. This means that all the phases are shifted 180° if they come from the negative film. The observed phases for the reflections $0\bar{4}0$, $02\bar{7}$ and 027 are 180, 0 and 180°, respectively, and they sum to 0°. These agree well with the prediction of direct methods.

In this study and our earlier investigation of $Ca_4Fe_2Ti_2O_{11}$ (Hovmöller, Zou, Wang, González-Calbet & Vallet-Regí, 1988), three-dimensional structures have been obtained from only one or two two-dimensional projections. This has been possible only because some additional knowledge of their basic structures has also been available (*e.g.* that the structures are perovskite related). However, HREM and CIP can also be applied to solve completely unknown inorganic structures. Several images from different crystal orientations would then have to be taken. The amplitudes and phases from these different images can be combined and a three-dimensional map can be calculated as demonstrated by Downing, Meisheng, Wenk & O'Keefe (1990). The procedure closely follows that used for solving unknown protein structures by EM and CIP (Hovmöller, Sjögren & Wang, 1988).

For superstructures caused by ordered vacancies with respect to their basic structures, the intensities of the superstructure reflections are entirely due to the vacancies. The intensities of the superstructure reflections are equal to what they could have been for a structure with a unit cell of the same size and empty, except for atoms at the vacancy positions. This can be used for identifying the true model out of several models, as in the present case. In the incorrect model, the vacancy lines are parallel and form a centered lattice. If this structure had been correct, superstructure reflections $0kl$ with $k+l=2n+1$ should be absent. Furthermore, the reflection 020 should be one of the strongest. However, the electron diffraction pattern of $Ba_2Fe_2O_5$ is not centred and 020 is a weak reflection. Therefore, this model was rejected. For the other model, with a weave-like arrangement of the vacancy lines, the calculated diffraction pattern agreed very well with the observed one. On this basis we concluded that this model is correct.

There are two steps in structure determination: solving the structure and refining it. HREM and CIP can be used for solving the structure, *i.e.* deducing atomic positions. This step is now much easier through the image-processing system *CRISP* running on a personal computer (Hovmöller, 1992). These atomic positions can then be refined, for example, by using diffraction amplitudes from a single crystal or powder or by energy minimization.

We have tried to obtain single crystals to confirm and refine the structure presented here by X-ray diffraction but unfortunately sufficiently large single crystals have not been obtained. The very large number of parameters in this structure (31 atoms, more than 100 parameters) is higher than the number of indexable lines (about 40) in the X-ray powder spectrum, so a refinement is not possible from powder data.

However, amplitudes from electron diffraction patterns can be used for the refinement. Electron diffraction usually extends to very high resolution (1 Å). The main problem for electron diffraction is multiple scattering. For superstructures, like the structure studied here, there are two categories of reflections: those from the basic structure and those from the superstructure. Of these, the former are heavily affected by multiple scattering, but the latter are not. The superstructure reflections may be considered kinematical even for quite thick crystals (>100 Å). Thus it should be possible to use the amplitudes obtained from electron diffraction in a least-square refinement, similar to X-ray crystallography. We are currently developing a system, called ELD, for measuring electron diffraction intensities quantitatively in order to refine the $Ba_2Fe_2O_5$ structure model (Zou & Hovmöller, 1992). A structure refinement by energy minimization is also in progress.

We thank the CICYT (Spain) and the Swedish Science Research Council (NFR) for financial support. SH acknowledges the Spanish Ministry of Education for a sabbatical grant.

References

BERTAUT, E. F., BLUM, P. & SAGNIÈRES, A. (1959). *Acta Cryst.* **12**, 149-159.
DOWNING, K. H., MEISHENG, H., WENK, H. R. & O'KEEFE, M. A. (1990). *Nature (London)*, **348**, 525-528.
ERCHARK, M., FANKUCHEN, J. I. & WARD, R. (1946). *J. Am. Chem. Soc.* **68**, 2085-2096.
GALLAGHER, P. K., MACCHESNEY, J. B. & BUCHANAN, D. N. E. (1965). *J. Chem. Phys.* **43**, 516-520.
GONZÁLEZ-CALBET, J. M., PARRAS, M., VALLET-REGÍ, M. & GRENIER, J. C. (1990). *J. Solid State Chem.* **86**, 149-159.
GRENIER, J. C., WATTIAUX, A., POUCHARD, M., HAGENMULLER, P., PARRAS, M., VALLET, M., GONZÁLEZ-CALBET, J. M. & ALARIO, M. (1989). *J. Solid State Chem.* **80**, 6-11.
HAUPTMAN, H. & KARLE, J. (1953). ACA Monograph No. 3. Ann Arbor: Edwards Brothers.
HOVMÖLLER, S. (1992). *Ultramicroscopy*, **41**, 121-135.
HOVMÖLLER, S., SJÖGREN, A., FARRANTS, G., SUNDBERG, M. & MARINDER, B.-O. (1984). *Nature (London)*, **311**, 238-241.
HOVMÖLLER, S., SJÖGREN, A. & WANG, D. N. (1988). *Prog. Biophys. Mol. Biol.* **51**, 131-163.
HOVMÖLLER, S., ZOU, X. D., WANG, D. N., GONZÁLEZ-CALBET, J. M. & VALLET-REGÍ, M. (1988). *J. Solid State Chem.* **77**, 316-321.
ICHIDA, T. (1973). *J. Solid State Chem.* **7**, 308-315.
LI, D. X. & HOVMÖLLER, S. (1988). *J. Solid State Chem.* **73**, 5-10.
LUCCINNI, E., MERIANI, S. & MINICHELLI, D. (1970). *Acta Cryst.* B**29**, 1217-1219.
MORI, S. (1965). *J. Am. Ceram. Soc.* **48**, 165.
NEGAS, T. & ROTH, R. (1969). *J. Res. Natl Bur. Stand. Sect. A*, **73**, 425-430.
PARRAS, M., FOURNES, L., GRENIER, J. C., POUCHARD, M., CALBET, J., VALLET, M. & HAGENMULLER, P. (1990). *J. Solid State Chem.* **88**, 261-268.
PARRAS, M., VALLET-REGÍ, M., GONZÁLEZ-CALBET, J. M., ALARIO, M. A., GRENIER, J. C. & HAGENMULLER, P. (1987). *Mater. Res. Bull.* **22**, 1413-1419.
RIETVELD, H. B. (1967). *Acta Cryst.* **22**, 151-152.
WANG, D. N., HOVMÖLLER, S., KIHLBORG, L. & SUNDBERG, M. (1988). *Ultramicroscopy*, **25**, 303-316.
ZANNE, M. (1973). PhD thesis, Univ. Nancy, France.
ZOU, X. D. & HOVMÖLLER, S. (1992). *Ultramicroscopy*. In the press.

Acta Cryst. (1993). A**49**, 35-45

Anisotropy of Anomalous Scattering in X-ray Diffraction. III. 'Forbidden' Axial Reflections in Space Groups up to Orthorhombic Symmetry

BY A. KIRFEL

Mineralogisches Institut, Universität Würzburg, Am Hubland, W-8700 Würzburg, Germany

AND W. MORGENROTH

Universität des Saarlandes, FR Kristallographie, W-6600 Saarbrücken 11, *Germany*

(*Received* 2 *September* 1991; *accepted* 18 *May* 1992)

Abstract

Kinematic single-crystal X-ray diffraction of totally polarized radiation is investigated for the presence of AAS (anisotropy of anomalous scattering). The developed model allows a clear distinction between geometric and structural aspects of the scattering. The former incorporates essentially an extension of the conventional polarization correction, the latter leads to a generalized structure factor. Both aspects are combined in the description of a structure-factor tensor that is defined in the diffractometer system and consists of a complex linear combination of six real basic tensors uniquely defining the dependence of a reflection intensity on both the scattering angle 2Θ and the azimuthal setting Ψ of the crystal. The complex coefficients of that structure-factor expansion are determined by the crystal structure, including the anisotropy of at least one atomic scattering factor. Under the limiting conditions of purely σ-polarized radiation and one 'edge atom' per asymmetric unit, effects of AAS on the systematically extinct ('forbidden') axial reflections in all monoclinic and orthorhombic space groups are studied. The compilation of the results offers both a concise survey over 23 unique cases of relevant symmetry and a practical guide to designing diffraction experiments. One possible application of FRED (forbidden reflection near-edge diffraction) is partial-structure determination, *i.e.* the location of an anisotropically resonant scattering 'edge atom' from the intensity variations $I(\mathbf{h}, \Psi)$. The method requires only AAS and a few reflections whose intensities are measured at selected azimuthal settings.

0108-7673/93/010035-11$06.00